Journal of Anatomy

J. Anat. (2017) **230**, pp461–470 doi: 10.1111/joa.12569

The effects of cracks on the quantification of the cancellous bone fabric tensor in fossil and archaeological specimens: a simulation study

Peter J. Bishop,[1,2,3] Christofer J. Clemente,[4] Scott A. Hocknull,[1,2,3] Rod S. Barrett[2,3,5] and David G. Lloyd[2,3,5]

[1]*Geosciences Program, Queensland Museum, Brisbane, Qld, Australia*
[2]*School of Allied Health Sciences, Griffith University, Southport, Qld, Australia*
[3]*Innovations in Health Technology, Menzies Health Institute Queensland, Gold Coast, Qld, Australia*
[4]*School of Science and Engineering, University of the Sunshine Coast, Maroochydore, Qld, Australia*
[5]*Gold Coast Orthopaedic Research and Education Alliance, Gold Coast, Qld, Australia*

Abstract

Cancellous bone is very sensitive to its prevailing mechanical environment, and study of its architecture has previously aided interpretations of locomotor biomechanics in extinct animals or archaeological populations. However, quantification of architectural features may be compromised by poor preservation in fossil and archaeological specimens, such as post mortem cracking or fracturing. In this study, the effects of post mortem cracks on the quantification of cancellous bone fabric were investigated through the simulation of cracks in otherwise undamaged modern bone samples. The effect on both scalar (degree of fabric anisotropy, fabric elongation index) and vector (principal fabric directions) variables was assessed through comparing the results of architectural analyses of cracked vs. non-cracked samples. Error was found to decrease as the relative size of the crack decreased, and as the orientation of the crack approached the orientation of the primary fabric direction. However, even in the best-case scenario simulated, error remained substantial, with at least 18% of simulations showing a $>10\%$ error when scalar variables were considered, and at least 6.7% of simulations showing a $>10^{\circ}$ error when vector variables were considered. As a 10% (scalar) or 10° (vector) difference is probably too large for reliable interpretation of a fossil or archaeological specimen, these results suggest that cracks should be avoided if possible when analysing cancellous bone architecture in such specimens.

Key words: cancellous bone; fabric tensor; fossils; simulation; taphonomic crack.

Introduction

Cancellous bone is a highly complex tissue found throughout the vertebrate skeleton. It is remarkable in its ability to adapt its structure to suit the prevailing mechanical environment, as demonstrated by *in vivo* experiments (Radin et al. 1982; Goldstein et al. 1991; Biewener et al. 1996; van der Meulen et al. 2006; Pontzer et al. 2006; Polk et al. 2008; Volpato et al. 2008; Barak et al. 2011) and computer simulations (Mullender & Huiskes, 1995; Huiskes et al. 2000; Adachi et al. 2001; Ruimerman et al. 2005; Wang et al. 2012). Further, studies of extant animal species have demonstrated that differences in locomotor behaviour often lead to differences in cancellous bone architecture (Fajardo & Müller, 2001; Ryan & Ketcham, 2002b, 2005; Maga et al. 2006; Hébert et al. 2012; Ryan & Shaw, 2012; Barak et al. 2013; Su et al. 2013; Tsegai et al. 2013; Matarazzo, 2015).

Given the sensitivity of cancellous bone to its mechanical environment, researchers have sometimes used cancellous bone architecture to help interpret locomotor biomechanics in extinct animals, or recently extinct human populations (Thomason, 1985; Macchiarelli et al. 1999; Ryan & Ketcham, 2002a; Ryan & Krovitz, 2006; Moreno et al. 2007; Gosman & Ketcham, 2009; DeSilva & Devlin, 2012; Barak et al. 2013; Su et al. 2013; Bishop et al. 2015; Chirchir et al. 2015; Ryan & Shaw, 2015; Skinner et al. 2015). Underpinning these studies is the quantification of various micro-structural characteristics of cancellous bone, such as bone volume fraction (a measure of porosity), trabecular thickness and spacing, and fabric direction or anisotropy (Odgaard & Gundersen, 1993; Odgaard, 1997, 2001; Ketcham & Ryan, 2004; Doube et al. 2010). These measures are typically made at fine spatial

Correspondence
Peter J. Bishop, Geosciences Program, Queensland Museum, 122 Gerler Road, Hendra, Qld 4011, Australia. E: peter.bishop@qm.qld.gov.au

Accepted for publication *24 October 2016*
Article published online *29 November 2016*

scales in the specimens, often approaching the continuum-scale (the scale at which the mechanical behaviour of a volume of cancellous bone can be replaced by a set of material properties that are averaged across the same volume). Each of the aforementioned studies has provided new insight that otherwise could not be obtained from the fossil or archaeological record. However, fossil and archaeological specimens may not be well preserved, on account of their age and the many environmental factors they can be subject to. A particularly common form of post mortem, taphonomic degradation is brittle deformation – cracking or fracturing – which can occur both before and after burial of the specimen (Behrensmeyer & Hill, 1980).

Macroscopic cracks that run through a fossil or archaeological specimen may potentially influence the results of a quantitative analysis of cancellous bone architecture, because they are features that are present in the specimen but were not there in the original, living bone. For instance, cracking of a fossil or archaeological specimen may sever trabecular connections, displace trabeculae relative to each other or introduce a void into the specimen (i.e. obliteration of actual bone structure). The presence of cracks could therefore confound interpretation, yet what influence they might have remains unknown. Further, if the presence of cracks does indeed influence the results of architectural analyses, it remains unknown as to whether this is true of all cracks, or only those of a certain size or shape. This is a potentially important problem, because essentially all fossil and archaeological specimens will have suffered macroscopic cracking to some degree, and the extent of cracking may not be able to be fully appreciated from visual examination of the specimen in hand sample. In previous studies of cancellous bone architecture in fossil or archaeological specimens, it is often unclear if the potential problems posed by cracks were addressed, perhaps because the studies' specimens (usually being of recent geological age) were indeed well preserved. One exception is the study of Ryan & Ketcham (2002a), who explicitly noted the presence of cracks in one specimen and moved their region of analysis away from the cracked region of bone. By and large, however, this approach of active identification and avoidance of cracks does not appear to have been followed in palaeontological and archaeological studies. It therefore remains that cracking in a fossil or archaeological specimen could present an impediment to the analysis and interpretation of cancellous bone architecture, especially in older fossil material that has the potential for greater taphonomic deformation.

The purpose of this study was to use computer simulations to elucidate the effects of crack size and orientation on the quantification of cancellous bone architecture in fossil and archaeological specimens. The approach was to analyse a variety of 'pristine' (undamaged) samples of modern cancellous bone, simulate the presence of cracks in those specimens and re-run the analyses, and compare the results for pristine vs. cracked specimens. The focus here is directed towards measures that describe the cancellous bone fabric tensor, because this strongly relates to the direction and stereotypy of *in vivo* loading (Fyhrie & Carter, 1987; Goldstein et al. 1991; Ryan & Ketcham, 2005; Pontzer et al. 2006; Barak et al. 2011).

Materials and methods

Image acquisition and processing

Ten samples of cancellous bone, derived from X-ray computed tomography (CT) scans of the limb bones of various modern avian and reptilian species, were studied (Table 1). The CT scans were acquired using either a Siemens Inveon (Siemens AG, Germany) or a GE BrightSpeed (GE Healthcare, UK); scan settings are detailed in Table 1. The scans were processed in the open-source software ImageJ 1.47 (http://imagej.nih.gov/ij/), and segmented using the local thresholding algorithm of Bernsen (1986), as implemented in ImageJ (Landini, 2008; Landini et al. 2016; see also Appendix). For the large bird bones scanned using the GE Brightspeed, the scans were resampled to isotropic voxels and at triple the original resolution using a bicubic interpolation algorithm; this did not alter the underlying structure in the scan data, but did facilitate a more effective segmentation of the cancellous bone. The samples for analysis were extracted as large cubes from the proximal and distal ends of the bones in the CT scans, and displayed a wide variety of structures.

Crack simulation

Cracks were simulated as planar prisms running through the middle of each sample at one of nine orientations (Fig. 1). These orientations were fixed relative to the orientation of the pre-determined fabric tensor for each specimen, such that four cracks were parallel to the primary fabric direction, one was perpendicular to the primary fabric direction, and four were at a 45° angle to the primary fabric direction (Fig. 1b). Although cracks can often assume a complex shape throughout a fossil or archaeological specimen, at the fine spatial scale at which cancellous bone architectural analyses are typically performed they can be reasonably approximated as planes. Moreover, the effect of cracks as simulated in this study was one of occlusion only: the cracks occluded the original cancellous bone structure in the CT scans, but did not introduce any new structure of their own (as might occur if high-density minerals precipitated along the internal surfaces of the crack). Crack geometry was initially defined in Rhinoceros 4.0 (McNeel, USA), and converted to voxels in an image stack using Mimics 17.0 (Materialize NV, Belgium). The voxels representing the crack were then subtracted from the CT scan image stack of the bone sample to simulate the obliteration of cancellous bone by the crack (Fig. 1e).

To investigate the effect of crack size on the results of an architectural analysis, a variety of crack thicknesses were simulated across the 10 samples. In absolute terms, these thicknesses ranged from 0.18 to 5.8 mm, which encompasses much of the range of macroscopic crack sizes that would be encountered in fossil or archaeological specimens. The thickness of the cracks was scaled to the mean trabecular spacing for each specimen, calculated using the method of Hildebrand & Rüegsegger (1997), as implemented in the BoneJ 1.3.11 plugin for ImageJ (Doube et al. 2010). Four thicknesses were tested, one-half, one, two and three times mean trabecular spacing. Only that part of the cancellous bone sample within a specified

Table 1 Samples of cancellous bone investigated in this study.

Sample	Collection number*	Description	Sample dimensions (mm)	Mean trabecular spacing (mm)	CT scan settings			
					Peak tube voltage (kV)	Tube current (mA)	Exposure time (ms)	Voxel resolution (mm)**
1	QMJ 48127	Saltwater crocodile (*Crocodylus porosus*) femoral head	10.653	0.399	80	0.45	1000	0.053
2	QMJ 48127	*Crocodylus porosus* medial femoral condyle	10.653	0.491	80	0.45	1000	0.053
3	PJB	Domestic chicken (*Gallus gallus*) femoral head	4.611	0.351	80	0.45	1000	0.053
4	QMJ 84416	Spencer's goanna (*Varanus spenceri*) proximal femur	7.473	0.694	80	0.5	900	0.053
5	AM R.106933	Komodo dragon (*Varanus komodoensis*) proximal tibia	7.473	0.590	80	0.45	1000	0.053
6	QMJ 47916	Australian freshwater crocodile (*Crocodylus johnstoni*) proximal tibia	5.247	0.505	80	0.5	900	0.053
7	QMO 30105	Southern cassowary (*Casuarius casuarius*) proximal tibiotarsus	14.673	0.811	120	55	1681	0.073 (0.219 × 0.3)
8	QMO 30105	*Casuarius casuarius* distal tibiotarsus	11.023	1.011	120	55	1681	0.073 (0.219 × 0.3)
9	MV R.2385	Ostrich (*Struthio camelus*) femoral head	24.613	1.482	120	55	1681	0.163 (0.488 × 0.3)
10	MV R.2385	*Struthio camelus* medial femoral condyle	18.093	1.949	120	55	1681	0.163 (0.488 × 0.3)

Samples 1–6 were CT scanned using a Siemens Inveon, and samples 7–10 were scanned using a GE BrightSpeed. Crack thicknesses were one-half, one, two and three times trabecular spacing; VOI diameter was five, nine and 13 times trabecular spacing (the last only possible for specimens 1, 2, 3, 7 and 9).

*Museum collection number abbreviations: QMJ, QMO, Queensland Museum Biodiversity Collections; AM R., Australian Museum Herpetology Collections, MV R., Museum Victoria Ornithology Collections; PJB, P.J.B. personal collection.

**Samples 7–10 were scanned with an anisotropic voxel resolution (original resolution in parentheses), and were resampled to an isotropic resolution.

volume of interest (VOI) was included in an analysis; the VOIs were defined as spheres centred at the centre of the cube, to avoid corner effects (Fig. 1d). Three VOI sizes were tested for both pristine and cracked samples, five, nine and 13 times mean trabecular spacing (the last only possible for five of the 10 specimens), each of which is sufficiently large for continuum-level analysis of cancellous bone architecture (Harrigan et al. 1988; Cowin, 2001). By scaling both crack thickness and VOI size to the intrinsic dimensions of each individual sample, this meant that constant ratios of crack thickness to VOI size were attained across the samples. Moreover, as the orientation of cracks was set up to be consistent with the intrinsic fabric of each individual sample, this also allowed for the effect of crack orientation to be investigated.

Architectural analyses

Analyses of cancellous bone architecture in pristine and cracked samples were conducted using the software Quant3D (Ryan & Ketcham, 2002a,b; Ketcham & Ryan, 2004). Two techniques that determine the fabric tensor (Cowin, 1986) were tested, the star volume distribution (SVD) and mean intercept length (MIL) methods; the MIL method in Quant3D was set to be the ellipsoid-based material tensor formulation. These are the two most widely used approaches in three-dimensional architectural analyses of cancellous bone, and the results of both have been demonstrated to show strong correlation with cancellous bone mechanical properties (Turner et al. 1990; Odgaard et al. 1997; Kabel et al. 1999; Ulrich et al. 1999). The SVD method essentially measures the spatial distribution (and in turn alignment) of bone material in a given volume, whereas the MIL method focuses on the distribution (and in turn alignment) of interfaces between the bone and non-bone phases in a given volume (Odgaard, 1997, 2001). For both methods, measurements were made for 2049 uniformly distributed orientations at 4000 points within the bone phase, with random rotation and dense vector sampling. (For the determination of the whole-sample fabric tensor, to guide the set-up of crack orientations, the SVD

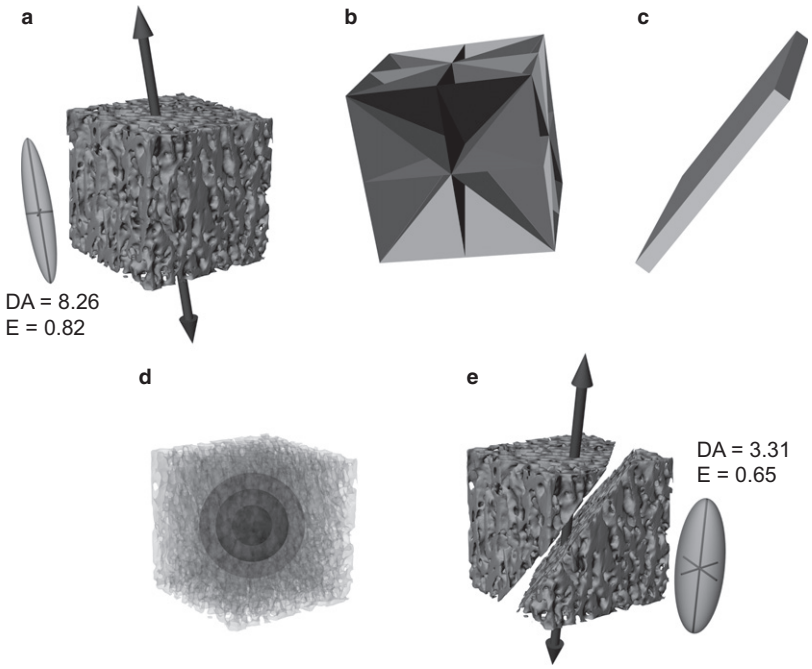

Fig. 1 The simulation of cracked specimens in this study. (a) A pristine sample of cancellous bone, from the proximal tibiotarsus of a cassowary, *Casuarius casuarius* (side length of cube = 14.673 mm). The large vector indicates the orientation of the primary fabric direction calculated for the whole sample, and the inset is the three-dimensional fabric ellipsoid (geometric expression of the fabric tensor) with associated measures (see text for explanation). (b) Nine standard orientations for the simulated cracks in this particular sample; all pass through the centre of the cube. Four planes are parallel to the primary fabric direction, one plane is perpendicular to it, and four planes are at a 45° angle to it. (c) One particular crack, simulated as a planar prism, here with thickness equal to twice the mean trabecular spacing of the sample. (d) Three spherical VOIs were used in the simulations, of diameter five, nine and 13 times the mean trabecular spacing. (e) The simulated cracked sample, where the cancellous bone in the volume of the crack in (c) has been removed, to simulate how a crack obliterates the structure. The resulting effect on the primary fabric orientation and nature of the fabric ellipsoid (and associated measures) is also illustrated.

method was used with the same parameters, on a sphere centred in the middle of the sample and occupying as large a volume as possible.) Upon calculation of the fabric tensor, the following variables were derived: the orientations of the primary, secondary and tertiary fabric directions (eigenvectors: $\mathbf{u}_1$, $\mathbf{u}_2$ and $\mathbf{u}_3$, respectively), the corresponding primary, secondary and tertiary fabric eigenvalues (e_1, e_2 and e_3, respectively), degree of fabric anisotropy (DA, calculated as e_1/e_3) and fabric elongation index (E, calculated as $1 - e_2/e_1$).

Comparing pristine and cracked samples

The effect of cracks was assessed by determining the mean ($\pm$ 1 SD) difference from the pristine sample, as a percentage for the scalar variables and as an angular deviation for the vector variables. This was computed for each combination of crack thickness and VOI size, and for each type of crack orientation (parallel, perpendicular or 45° to the orientation of $\mathbf{u}_1$). Angular deviation between the orientation of vectors in a cracked and pristine sample was calculated using the dot product of the two vectors:

$$\theta_{\text{cracked}-\text{pristine}} = \arccos\left(\frac{\mathbf{v}_{\text{cracked}} \bullet \mathbf{v}_{\text{pristine}}}{|\mathbf{v}_{\text{cracked}}| \times |\mathbf{v}_{\text{pristine}}|}\right)$$

Additionally, the frequency of unacceptably large differences was investigated. An unacceptably large difference is one where an error of that magnitude in the real world would confound interpretation of a fossil or archaeological specimen. Thus, an *a priori* maximum acceptable difference was set for each scalar and vector variable examined, and the proportion of instances in which the difference between cracked and pristine samples exceeded that limit, $P(\Delta_{max})$, was determined for each combination of VOI size and crack thickness and for each type of crack orientation. For scalar variables, this limit was $\pm$ 10% of the value determined for the pristine sample. For vector variables, the limit was a 10° cone around the vector determined for the pristine sample. These limits were chosen based on the results of previous studies, which have shown that distinct locomotor differences in species can manifest themselves as architectural differences of these magnitudes, or even less (Ryan & Ketcham, 2002b; Maga et al. 2006; Pontzer et al. 2006; Polk et al. 2008; Griffin et al. 2010; Barak et al. 2013; Su et al. 2013; Tsegai et al. 2013). Hence, errors in measurement of 10% (for scalar variables) or 10° (for vector variables) could be large enough to preclude reliable and in-depth interpretation of a fossil or archaeological specimen.

Results

Scalar variables – DA and *E*

Attention is only given to the degree of anisotropy (DA) and elongation index (E) here, because the individual

eigenvalues of a fabric tensor are not meaningful in their own right; it is only when expressed relative to each other (in measures such as DA and *E*) that they are informative (Ryan & Ketcham, 2002b; Maga et al. 2006; Hébert et al. 2012; Matarazzo, 2015). In both the SVD and MIL analyses, both the mean positive differences (where the cracked value was greater than the pristine value) and mean negative differences (where the cracked value was less than the pristine value) tended to decrease as the ratio of crack thickness to VOI size decreased (Fig. 2a). The margin of error about these means also tended to decrease as the ratio of crack thickness to VOI size decreased, although it is important to note that even at the lowest ratio tested (1/26 or 3.8%) the margin of error often remained considerable, with a standard deviation usually in excess of 10%. The proportion of instances in which the maximum acceptable difference for both DA and *E* was exceeded, $P(\Delta_{max})$, generally decreased as the ratio of crack thickness to VOI size decreased, for both SVD and MIL analyses (Fig. 2b). Even at the lowest ratio tested, however, $P(\Delta_{max})$ was at least 0.18; that is, there was essentially a one-in-six chance or greater that a measurement for a cracked sample was more than 10% in error of that calculated for the pristine sample.

Vector variables – principal fabric directions

The mean angular difference between the vector orientations of cracked and pristine samples tended to decrease as the ratio of crack thickness to VOI size decreased, for all three fabric directions and for both SVD and MIL methods (Fig. 3a). The margin of error about the mean also tended to decrease as the ratio of crack thickness to VOI size decreased, although again it remained considerable even for the lowest ratio tested, with the standard deviation being at least 6°, and often in excess of 10°. As with the scalar variables, $P(\Delta_{max})$ generally decreased as the ratio of crack thickness to VOI size decreased (Fig. 3b). However, $P(\Delta_{max})$ remained above 0.16 in all SVD analyses, and in the MIL analyses it typically remained above 0.11; only at the lowest ratio of crack thickness to VOI size was a lower value observed (0.067), and this was only in regards to the orientation of $\mathbf{u}_1$. Thus, for the SVD analyses, there was

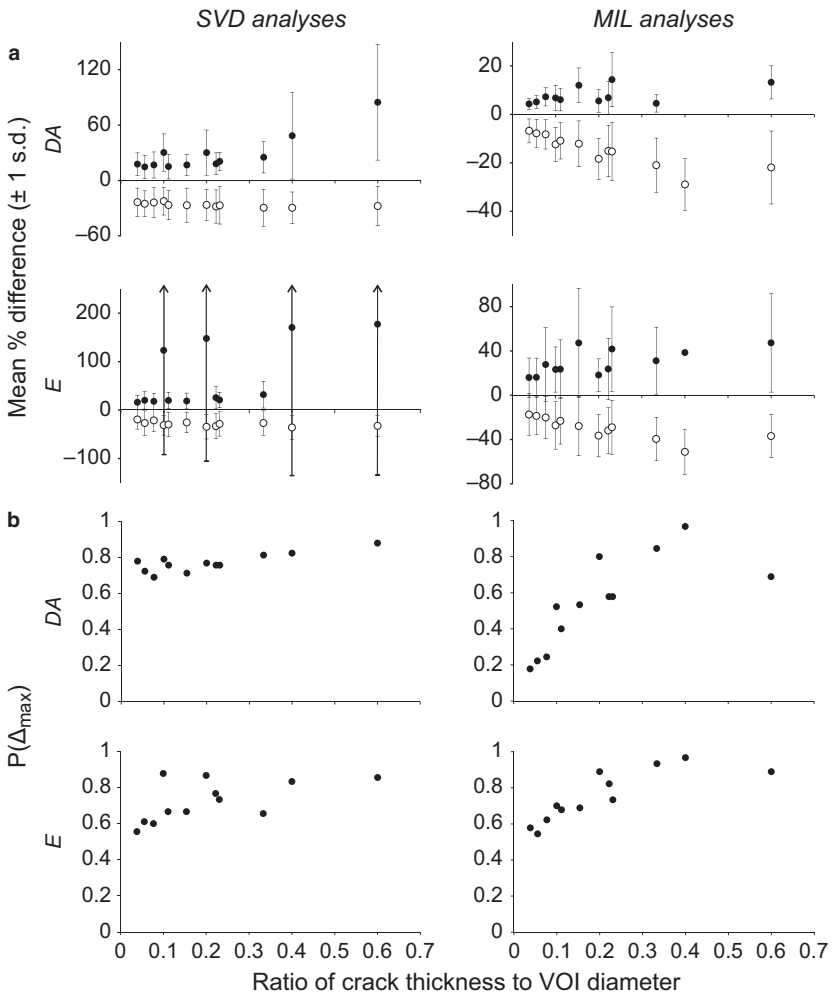

Fig. 2 The effect of cracks on scalar variables describing the cancellous bone fabric tensor. (a) In terms of the mean percentage difference from the pristine sample. (b) In terms of $P(\Delta_{max})$, the proportion of instances where the maximum acceptable difference was exceeded. For the mean difference plots, filled circles denote positive differences from the values for the pristine sample, and hollow circles denote negative differences from the values for the pristine sample.

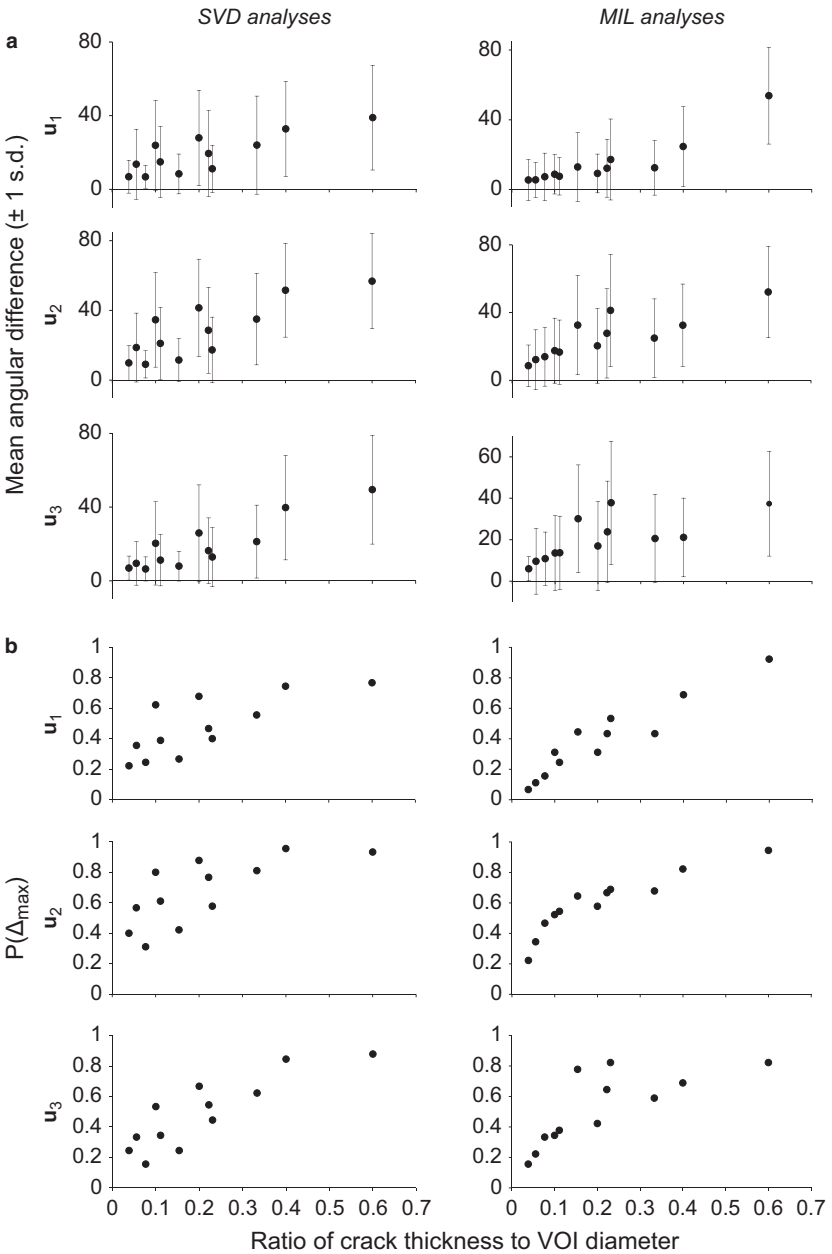

Fig. 3 The effect of cracks on vector variables describing the cancellous bone fabric tensor. (a) In terms of the angular differences from the pristine sample. (b) In terms of $P(\Delta_{max})$, the proportion of instances where the maximum acceptable difference was exceeded.

essentially a one-in-six chance or greater that a vector orientation calculated for a cracked sample was more than 10° off that calculated for the pristine sample. Furthermore, for the MIL analyses, there was essentially a one-in-10 chance or greater that a vector orientation calculated for a cracked sample was in error of 10° or more, except at the lowest ratio of crack thickness to VOI size.

The effect of crack orientation

Crack orientation had a largely consistent effect on the results for both scalar and vector variables, calculated with both SVD and MIL methods (Fig. 4a,b). Overall, the error decreased as the crack orientation became more parallel to the orientation of the primary fabric direction, $\mathbf{u}_1$. There were a few exceptions to this general pattern (two of which are illustrated in Fig. 4c,d); in these cases, error tended to increase as the crack approached being parallel to $\mathbf{u}_1$, although this was typically only slight.

Discussion

The simulations performed in this study sought to examine the effect of including cracks in a VOI on the quantitative analysis of cancellous bone architecture. It was found that, in general, as the size (thickness) of the crack relative to the

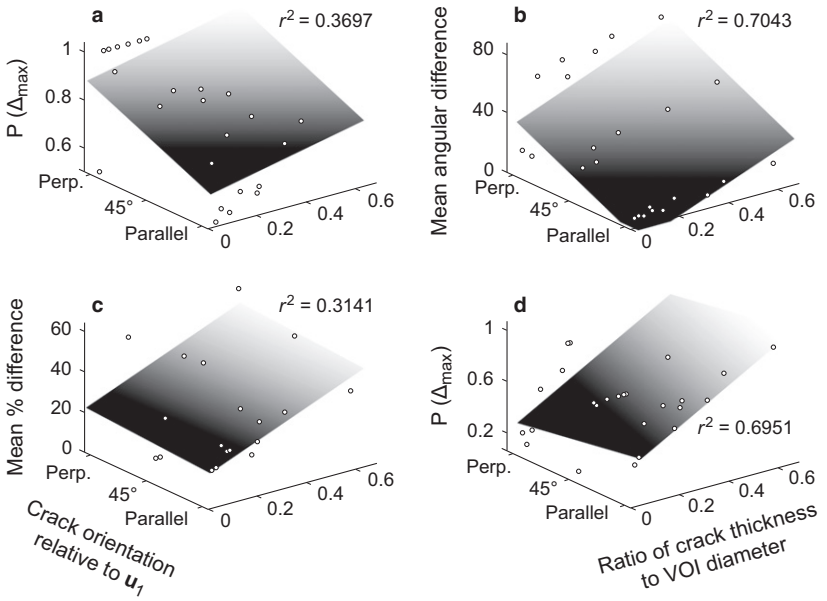

Fig. 4 The effect of crack orientation on the quantification of the cancellous bone fabric tensor, as illustrated with several exemplar cases. These three-dimensional plots tease apart the general patterns shown in Figs 2 and 3, to illustrate how crack orientation (relative to the primary fabric direction) also influences the results of quantitative analysis. (a) Proportion of excessively erroneous instances for degree of anisotropy in SVD analyses. (b) Mean angular difference for the orientation of the primary fabric direction in SVD analyses. (c) Mean percentage difference for positive error in elongation index in MIL analyses. (d) Proportion of excessively erroneous instances for the orientation of the secondary fabric direction in MIL analyses. By and large, the general pattern was that demonstrated in (a) and (b), where error markedly decreases as the crack becomes more parallel to the orientation of the primary fabric direction, although exceptions did exist, as illustrated in (c) (little decrease with more parallel orientation) and (d) (slight increase with more parallel orientation). For illustrative purposes, planes were fitted to the data (and associated r^2 values calculated) assuming a coding of parallel orientation = 1, 45° orientation = 2, perpendicular orientation = 3, using the Curve Fitting Toolbox in MATLAB (version 8.0, MathWorks, Natick, MA, USA).

size of the VOI decreased, so too did the mean difference between pristine and cracked samples, in terms of both scalar (fabric anisotropy and elongation index) and vector (principal fabric directions) variables. The margin of error about the mean also tended to decrease as relative crack size decreased. As a consequence, the proportion of instances in which the maximum acceptable difference was exceeded, $P(\Delta_{max})$, also tended to decrease as relative crack size decreased, although the decrease for the scalar variables tended to be only slight. This result was expected, as the crack is occupying a smaller proportion of the total volume of cancellous bone being analysed, and thus obscuring less of the actual structure. The orientation of a crack relative to the underlying cancellous bone fabric was also shown to have an influence on the magnitude of error encountered; in general, as the crack became more parallel to the primary fabric direction ($\mathbf{u}_1$), the error decreased.

Despite these trends, even at the smallest relative size of crack tested (crack thickness = 3.8% of VOI diameter, and VOI diameter many times greater than trabecular spacing), the magnitude of error often remained substantial, when both mean difference and error about the mean are taken into consideration. Furthermore, $P(\Delta_{max})$ was still considerable, *at least* 18% for scalar variables and *at least* 11% for the orientation of principal fabric directions (with the exception of the direction of $\mathbf{u}_1$ in MIL analyses, for which it was 6.7%). That is, there was still a considerable probability that calculated scalar parameters were more than 10% off their true value, and calculated vectors were more than 10° off their true orientation. This sizeable degree of uncertainty and error involved would hence effectively preclude meaningful interpretation of the specimen. Although the present study did not simulate cracks finer than 0.18 mm across (or finer than one-half mean trabecular spacing), the trends observed in Figs 2 and 3 suggest that even at smaller crack thicknesses, there may still be significant potential for error.

Before drawing any conclusions, it is important to bear in mind the limitations of the current study. For the sake of simplicity, cracks were simulated under a particular set of assumptions regarding shape (planar geometry), extent (extending the whole way through a VOI) and number (only a single crack in a given VOI), and their effect was assumed to be of occlusion only. More complex crack manifestations were not investigated. Moreover, all analyses were made at fine to medium spatial scales; the effect of cracks on the analysis of large VOIs that occupy a large portion of an articular condyle, for example (as in the studies of Ryan & Walker, 2010; Scherf et al. 2013), remains untested. It is

conceivable that variations in the above parameters could have different effects on the results of quantitative analysis, but this would need to be the subject of further, more detailed study. An additional complexity is the possibility of differential displacement of otherwise well-preserved portions of cancellous bone on either side of a crack.

Notwithstanding these factors, the results of this study do suggest that caution should be exercised when quantitatively analysing cancellous bone architecture in fossil or archaeological specimens. When selecting specimens for cancellous bone architectural analysis, the best approach would be to carefully inspect potential specimens for cracking (using a magnifying glass or microscope if necessary), and select the specimen or specimens that have suffered the least amount of taphonomic degradation. In some situations, it may be possible for a researcher to visually identify cracks from even the finer end of the thickness spectrum investigated in the present study, and thus immediately reject a specimen from consideration. However, a number of complicating factors can exist. Most importantly, cracks may be present within the specimen that have not yet reached the surface: these cracks are invisible to the researcher until the bone is actually CT scanned. Secondly, fine hairline cracks at the surface, which may be able to be easily seen in relatively young specimens, may be less easily discerned in older fossils, especially if they are obscured by matrix, consolidant or other material. Thirdly, the researcher may not always have multiple specimens among which to choose the best specimen for study; for example, if there is only one femur specimen known for a given extinct species, then that specimen would have to be studied if anything is to be learnt at all for that species. It is therefore of great importance to not only visually inspect a potential specimen for cracking in hand sample, but to also inspect the resulting CT scans before attempting a quantitative analysis. Ideally, even if cracks are found to be present, they should be avoided in a VOI for analysis, regardless of their size or the method used to quantify the cancellous architecture. If this is not feasible, for instance for the purposes of achieving a consistently positioned VOI in comparative studies (Fajardo & Müller, 2001; Kivell et al. 2011), then the VOI used should be as large as possible, although this may in turn introduce bias through inconsistent VOI sizes used across samples (Kivell et al. 2011; Lazenby et al. 2011).

Acknowledgements

Sincere appreciation is extended to Ms H. Janetzki, Mr P.J. Couper, Dr A. Amey (Queensland Museum), Dr K.K. Roberts (Museum Victoria) and Dr R. Sadlier (Australian Museum) for the loan of specimens, and to Dr K. Mardon (University of Queensland Centre for Advanced Imaging) and Mr I. Mitchell (Queensland X-Ray) for performing the CT scanning. The thoughtful and constructive comments of two anonymous reviewers, and the editor, are also greatly appreciated. This research was supported by an Australian Postgraduate Award (to P.J.B.), an Australian Research Council DECRA Fellowship (DE120101503, to C.J.C.) and the donation of CT scan time by Queensland X-Ray (to S.A.H.). The authors declare no conflict of interests.

Author contributions

P.J.B., R.S.B. and D.G.L. conceived the study design. P.J.B., C.J.C. and S.A.H. collected CT scan data. All authors contributed to data analysis, interpretation and drafting of the manuscript. All authors approved the final draft.

References

Adachi T, Tsubota K, Tomita Y, et al. (2001) Trabecular surface remodeling simulation for cancellous bone using microstructural voxel finite element models. *J Biomech Eng* **123**, 403–409.

Barak MM, Lieberman DE, Hublin J-J (2011) A Wolff in sheep's clothing: trabecular bone adaptation in response to changes in joint loading orientation. *Bone* **49**, 1141–1151.

Barak MM, Lieberman DE, Raichlen DA, et al. (2013) Trabecular evidence for a human-like gait in *Australopithecus africanus*. *PLoS ONE* **8**, e77687.

Behrensmeyer AK, Hill AP (1980) *Fossils in the Making Vertebrate Taphonomy and Paleoecology*. Chicago: University of Chicago Press.

Bernsen J (1986) Dynamic thresholding of grey-level images. *Proceedings of the 8th International Conference on Pattern Recognition*, pp. 1251–1255. Paris: France.

Biewener AA, Fazzalari NL, Konieczynski DD, et al. (1996) Adaptive changes in trabecular architecture in relation to functional strain patterns and disuse. *Bone* **19**, 1–8.

Bishop PJ, Walmsley CW, Phillips MJ, et al. (2015) Oldest pathology in a Tetrapod Bone illuminates the origin of terrestrial vertebrates. *PLoS ONE* **10**, e0125723.

Chirchir H, Kivell TL, Ruff CB, et al. (2015) Recent origin of low trabecular bone density in modern humans. *Proc Natl Acad Sci* **112**, 366–371.

Cowin SC (1986) Wolff's law of trabecular architecture at remodelling equilibrium. *J Biomech Eng* **108**, 83–88.

Cowin SC (2001) The false premise in Wolff's Law. In: *Bone Biomechanics Handbook*. (ed. Cowin SC), pp. 30-1–30-15. Boca Raton: CRC Press.

DeSilva JM, Devlin MJ (2012) A comparative study of the trabecular bony architecture of the talus in humans, non-human primates, and *Australopithecus*. *J Hum Evol* **63**, 536–551.

Doube M, Kłosowski MM, Arganda-Carreras I, et al. (2010) BoneJ: free and extensible bone image analysis in ImageJ. *Bone* **47**, 1076–1079.

Fajardo RJ, Müller R (2001) Three-dimensional analysis of nonhuman primate trabecular architecture using micro-computed tomography. *Am J Phys Anthropol* **115**, 327–336.

Fyhrie DP, Carter DR (1987) A unifying principle relating stress to trabecular bone morphology. *J Orthop Res* **4**, 304–317.

Goldstein SA, Matthews LS, Kuhn JL, et al. (1991) Trabecular bone remodelling: an experimental model. *J Biomech* **24** (Suppl. 1), 135–150.

Gosman JH, Ketcham RA (2009) Patterns in ontogeny of human trabecular bone from SunWatch Village in the Prehistoric Ohio Valley: general features of microarchitectural change. *Am J Phys Anthropol* **138**, 318–332.

Griffin NL, D'Août K, Ryan TM, et al. (2010) Comparative forefoot trabecular bone architecture in extant hominids. *J Hum Evol* **59**, 202–213.

Harrigan TP, Jasty M, Mann RW, et al. (1988) Limitations of the continuum assumption in cancellous bone. *J Biomech* **21**, 269–275.

Hébert D, Lebrun R, Marivaux L (2012) Comparative three-dimensional structure of the trabecular bone in the talus of primates and its relationship to ankle joint loads generated during locomotion. *Anat Rec* **295**, 2069–2088.

Hildebrand T, Rüegsegger P (1997) A new method for the model-independent assessment of thickness in three-dimensional images. *J Microsc* **185**, 67–75.

Huiskes R, Ruimerman R, van Lenthe GH, et al. (2000) Effects of mechanical forces on maintenance and adaptation of form in trabecular bone. *Nature* **405**, 704–706.

Kabel J, van Rietbergen B, Odgaard A, et al. (1999) Constitutive relationships of fabric, density, and elastic properties in cancellous bone architecture. *Bone* **25**, 481–486.

Ketcham RA, Ryan TM (2004) Quantification and visualization of anisotropy in trabecular bone. *J Microsc* **213**, 158–171.

Kivell TL, Skinner MM, Lazenby R, et al. (2011) Methodological considerations for analyzing trabecular architecture: an example from the primate hand. *J Anat* **218**, 209–225.

Landini G (2008) Advanced shape analysis with ImageJ. In: *Proceedings of the Second ImageJ User and Developer Conference*. pp. 116–121. Luxembourg: The Centre de Recherche Public Henri Tudor.

Landini G, Randell DA, Fouad S, et al. (2016) Automatic thresholding from the gradients of region boundaries. *J Microsc*. In Press.

Lazenby R, Skinner MM, Kivell TL, et al. (2011) Scaling VOI Size in 3D μCT studies of trabecular bone: a test of the over-sampling hypothesis. *Am J Phys Anthropol* **144**, 196–203.

Macchiarelli R, Bondioli L, Galichon V, et al. (1999) Hip bone trabecular architecture shows uniquely distinctive locomotor behaviour in South African australopithecines. *J Hum Evol* **36**, 211–232.

Maga M, Kappelman J, Ryan TM, et al. (2006) Preliminary observations on the calcaneal trabecular microarchitecture of extant large-bodied hominoids. *Am J Phys Anthropol* **129**, 410–417.

Matarazzo SA (2015) Trabecular architecture of the manual elements reflects locomotor patterns in primates. *PLoS ONE* **10**, e0120436.

van der Meulen MCH, Morgan TG, Yang X, et al. (2006) Cancellous bone adaptation to *in vivo* loading in a rabbit model. *Bone* **38**, 871–877.

Moreno K, Carrano MT, Snyder R (2007) Morphological changes in pedal Phalanges through ornithopod dinosaur evolution: a biomechanical approach. *J Morphol* **268**, 50–63.

Mullender MG, Huiskes R (1995) Proposal for the regulatory mechanism of Wolff's law. *J Orthop Res* **13**, 503–512.

Odgaard A (1997) Three-dimensional methods for quantification of cancellous bone architecture. *Bone* **20**, 315–328.

Odgaard A (2001) Quantification of cancellous bone architecture. In: *Bone Biomechanics Handbook*. (ed. Cowin SC), pp. 14-1–14-19. Boca Raton: CRC Press.

Odgaard A, Gundersen HJG (1993) Quantification of connectivity in cancellous bone, with special emphasis on 3-D reconstructions. *Bone* **14**, 173–182.

Odgaard A, Kabel J, van Rietbergen B, et al. (1997) Fabric and elastic principal directions of cancellous bone are closely related. *J Biomech* **30**, 487–495.

Polk JD, Blumenfeld J, Ahluwalia D (2008) Knee posture predicted from subchondral apparent density in the distal femur: an experimental validation. *Anat Rec* **16**, 323–329.

Pontzer H, Lieberman DE, Momin E, et al. (2006) Trabecular bone in the bird knee responds with high sensitivity to changes in load orientation. *J Exp Biol* **209**, 57–65.

Radin EL, Orr RB, Kelman JL, et al. (1982) Effect of prolonged walking on concrete on the knees of sheep. *J Biomech* **15**, 487–492.

Ruimerman R, Hilbers P, van Rietbergen B, et al. (2005) A theoretical framework for strain-related trabecular bone maintenance and adaptation. *J Biomech* **38**, 931–941.

Ryan TM, Ketcham RA (2002a) Femoral head trabecular bone structure in two omomyid primates. *J Hum Evol* **43**, 241–263.

Ryan TM, Ketcham RA (2002b) The three-dimensional structure of trabecular bone in the femoral head of strepsirrhine primates. *J Hum Evol* **43**, 1–26.

Ryan TM, Ketcham RA (2005) Angular orientation of trabecular bone in the femoral head and its relationship to hip joint loads in leaping primates. *J Morphol* **265**, 249–263.

Ryan TM, Krovitz GE (2006) Trabecular bone ontogeny in the human proximal femur. *J Hum Evol* **51**, 591–602.

Ryan TM, Shaw CN (2012) Unique suites of trabecular bone features characterize locomotor behavior in human and non-human anthropoid primates. *PLoS ONE* **7**, e41037.

Ryan TM, Shaw CN (2015) Gracility of the modern *Homo sapiens* skeleton is the result of decreased biomechanical loading. *Proc Natl Acad Sci* **112**, 372–377.

Ryan TM, Walker A (2010) Trabecular bone structure in the humeral and femoral heads of anthropoid primates. *Anat Rec* **293**, 719–729.

Scherf H, Harvati K, Hublin J-J (2013) A comparison of proximal humeral cancellous bone of great apes and humans. *J Hum Evol* **65**, 29–38.

Skinner MM, Stephens NB, Tsegai ZJ, et al. (2015) Human-like hand use in Australopithecus africanus. *Science* **347**, 395–399.

Su A, Wallace IJ, Nakatsukasa M (2013) Trabecular bone anisotropy and orientation in an Early Pleistocene hominin talus from East Turkana, Kenya. *J Hum Evol* **64**, 667–677.

Thomason JJ (1985) The relationship of trabecular architecture to inferred loading patterns in the third metacarpals of the extinct equids *Merychippus* and *Mesohippus*. *Paleobiology* **11**, 323–335.

Tsegai ZJ, Kivell TL, Gross T, et al. (2013) Trabecular bone structure correlates with hand posture and use in hominoids. *PLoS ONE* **8**, e78781.

Turner CH, Cowin SC, Rho JY, et al. (1990) The fabric dependence of the orthotropic elastic constants of cancellous bone. *J Biomech* **23**, 549–561.

Ulrich D, van Rietbergen B, Laib A, et al. (1999) The ability of three-dimensional structural indices to reflect mechanical aspects of trabecular bone. *Bone* **25**, 55–60.

Volpato V, Viola TB, Nakatsusaka M, et al. (2008) Textural characteristics of the iliac-femoral trabecular pattern in a bipedally trained Japanese macaque. *Primates* **49**, 16–25.

Wang H, Ji B, Liu XS, et al. (2012) Analysis of microstructural and mechanical alterations of trabecular bone in a simulated three-dimensional remodelling process. *J Biomech* **45**, 2417–2425.

Appendix

In this study, the CT scans were segmented using the algorithm of Bernsen (1986), as implemented in ImageJ (Landini, 2008; Landini et al. 2016; note that the implementation operates on 8-bit images only). This algorithm is a binary pixel classifier, identifying whether a given pixel in an image belongs to the foreground (bone tissue, assigned a value of 1) or background (intertrabecular spaces, assigned a value of 0). Moreover, it takes into consideration only pixels within the focal pixel's local neighbourhood (a 'window of interest'), the size of which is given by a pre-specified radius. By considering an image in terms of local regions, and moving the window of interest from pixel to pixel, this approach can overcome variations in brightness or contrast across an image, which can present difficulties to global thresholding approaches that consider an entire image simultaneously. The steps used by the algorithm for each pixel are as follows.

1 Calculate the local contrast (C_{local}) of the pixels within the local neighbourhood of the focal pixel, equal to the difference between maximum and minimum grey values in the neighbourhood: $C_{local} = value_{max} - value_{min}$.
2 If C_{local} equals or exceeds a pre-specified contrast threshold (C_{thresh}), then the segmenting threshold is set as the mid-grey value of the pixels within the local neighbourhood, which is the average of the maximum and minimum grey values in the neighbourhood: $M = ½(value_{max} + value_{min})$. This is then used to classify the focal pixel as either belonging to the foreground ($value_{focal} \geq M$) or background ($value_{focal} < M$).
3 If C_{local} is less than C_{thresh}, then the focal pixel is classified according to whether the mid-grey value of the pixels in the local neighbourhood is brighter or darker than the mid-point of the 8-bit spectrum: if $M \geq 128$, it belongs to the foreground, if $M < 128$, it belongs to the background.

The exact values for the window radius and contrast threshold used to segment the scans in the present study varied from specimen to specimen, and were chosen based on visual comparison of the original vs. segmented scans.